Gondwana Research 116 (2023) 104–112

Contents lists available at ScienceDirect

Gondwana Research

journal homepage: www.elsevier.com/locate/gr

GR Letter

The late Cenozoic evolution of the Humboldt Current System in coastal Peru: Insights from neodymium isotopes

Steffen Kiel [a,*], Michal Jakubowicz [b], Alí Altamirano [c], Zdzislaw Belka [b], Jolanta Dopieralska [d], Mario Urbina [c], Rodolfo Salas-Gismondi [c,e]

[a] Swedish Museum of Natural History, Department of Palaeobiology, Box 50007, 10405 Stockholm, Sweden
[b] Isotope Research Unit, Adam Mickiewicz University, 61-680 Poznań, Poland
[c] Museo de Historia Natural, Universidad Nacional Mayor San Marcos (MUSM), Departamento de Paleontología de Vertebrados, Av. Arenales 1256, Lima, Peru
[d] Poznan Science and Technology Park, Adam Mickiewicz University Foundation, 61-612 Poznań, Poland
[e] Universidad Peruana Cayetano Heredia, Facultad de Ciencias y Filosofía y Centro de Investigación para el Desarrollo Integral y Sostenible (CIDIS), Paleontología y Evolución de Vertebrados Lab, Lima, Peru

ARTICLE INFO

Article history:
Received 15 March 2022
Revised 28 November 2022
Accepted 31 December 2022
Available online 5 January 2023
Handling Editor: R.D. Nance

Keywords:
Paleoceanography
Miocene
Biogenic bloom
permanent El Niño
South America

ABSTRACT

The Humboldt Current System along the Pacific coast of South America creates one of the most productive ecosystems on Earth. To trace the origin of the water masses in this area, we measured neodymium isotope compositions (ε_{Nd}) in tooth enameloid of two genera of coastal sharks from latest Oligocene to early Pleistocene strata in the Pisco and Sacaco basins in southern Peru. Most ε_{Nd} values range from −4 to −1, with a strong negative excursion in the late Miocene (~8–7 million years ago [Ma]) with values as low as −9.2. The overall trend of the ε_{Nd} values resembles that of equatorial Pacific deep waters, though with an offset of about +2 ε_{Nd} units until about 6 Ma. With a major input of hinterland weathering considered unlikely, we interpret this pattern as reflecting a modern-type upwelling regime, though with a lower contribution of Antarctic waters than today. Starting about 6 Ma, the contribution of Antarctic waters to the upwelling waters increased approximately to present-day levels, coincident with, and possibly driven by, increased Antarctic glaciation and the Andes reaching their present-day elevation, both of which likely enhanced the counter-clockwise circulation in the South Pacific Ocean. The negative excursion of ε_{Nd} values in the Pisco/Sacaco basins ~8–7 Ma coincides with a late Miocene biogenic bloom in the Pacific Ocean and elsewhere, and with a strongly increased northward bottom current observed on the Nazca Drift System just offshore our sampling area. Thus, the negative excursion of ε_{Nd} values in the Pisco/Sacaco basins likely resulted from a southern sourced input of nutrient-rich, unradiogenic water, which could have been an important contributor to the biogenic bloom.

1. Introduction

The Humboldt Current System comprises the surface and subsurface flows in the eastern boundary current system along the Pacific coast of South America (Fig. 1). The upwelling of cold, nutrient-rich waters along the coast of Peru and Chile creates one of the most productive ecosystems on Earth, producing more fish per unit area than any other region, and about 10 % of the world's fish catch (Thiel et al., 2007; Chavez et al., 2008; Montecino and Lange, 2009). Through the decay of the abundant organic matter and the oxygen-poor nature of the upwelling water, it also results in one of the world's largest and shallowest Oxygen Minimum Zones (Helly and Levin, 2004). Upwelling is driven by equatorward surface winds along the Peruvian coast, leading to Ekman transport offshore and thus upwelling along the coast. The upwelling water masses are composed of the underlying waters of the poleward Peru-Chile Undercurrent (PCUC), Sub-Antarctic Mode Water (SAMW) and local recirculation (Fig. 1; Karstensen and Ulloa, 2009; Montes et al., 2010; Grasse et al., 2012; Toggweiler et al., 2019).

Whereas the short-term variability of this upwelling system, for example the El Niño–southern Oscillation phenomenon or Ice Age-related changes, are well studied (Salvatteci et al., 2016; Timmermann et al., 2018), much is still to be learned about its longer-term evolution. Its origin was linked to the onset of the Antarctic Circumpolar Current (ACC) in the Eocene

* Corresponding author.
E-mail address: steffen.kiel@nrm.se (S. Kiel).

https://doi.org/10.1016/j.gr.2022.12.008
1342-937X/

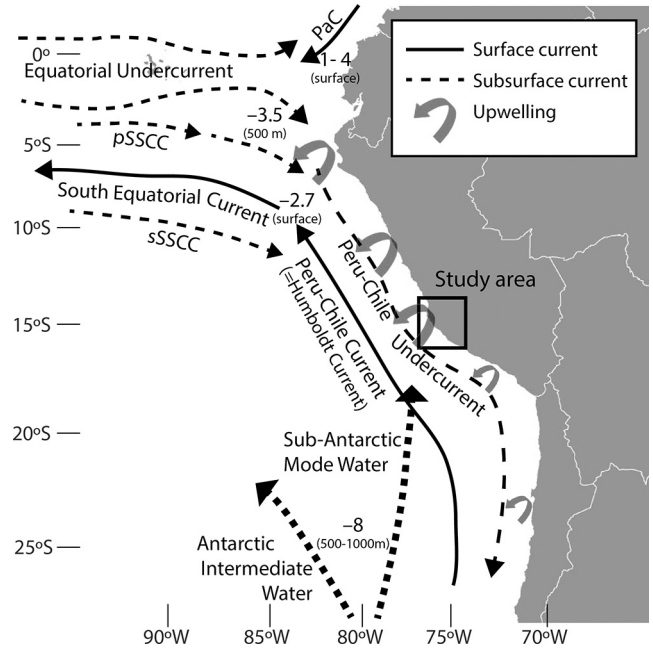

Fig. 1. Schematic oceanography off northwestern South America and ε_{Nd} values of key ocean currents and water masses (after: Karstensen and Ulloa, 2009; Montecino and Lange, 2009; Grasse et al., 2012; Bostock et al., 2013; Basak et al., 2015; Grasse et al., 2017). PaC: Panama Current; pSSCC and sSSCC: primary and secondary Southern Subsurface Countercurrent.

(Marty et al., 1988), and upwelling analogous to the present-day condition were suggested to have persisted since then (von Huene et al., 1987; Lagabrielle et al., 2009; Armijo et al., 2015; DeVries et al., 2017). However, paleontological studies in the Pisco and Sacaco basins suggest a more complex history (Muizon and Devries, 1985; Collareta et al., 2021; Ochoa et al., 2021). They indicate the persistence of warm-water faunas well into the Neogene (Bosio et al., 2020), marked changes in diversity in the latest Miocene-early Pliocene, and faunal communities resembling those of the present-day Humboldt Current System only from the late Pliocene onward (Ochoa et al., 2021).

Biogenic phosphates are among the most commonly used archives of the Nd isotope composition of seawater for past oceans (Staudigel et al., 1985; Martin and Haley, 2000; Dopieralska et al., 2016). While vertebrate bones may be subjected to substantial diagenetic exchange that compromises their utility as a seawater ε_{Nd} archive (Kocsis et al., 2010; Tütken et al., 2011), fluorapatite forming fish (including shark) teeth, and most notably the enamel and enameloid, show high resistance to late-diagenetic alteration, providing a reliable recorder of seawater Nd isotope signatures for Cenozoic timescales (e.g., Scher and Martin, 2006; Kocsis et al., 2010; Scher and Delaney, 2010; Moiroud et al., 2013; Kim et al., 2020). The MREE-enriched patterns commonly observed in fish teeth reflect acquiring their REEs largely from shallow-level, early-diagenetic pore waters, rather than directly from seawater; in most cases, fish-tooth fluorapatite can, however, be expected to reflect the seawater ε_{Nd} signal (Martin and Haley, 2000; Kocsis et al., 2010; Huck et al., 2016). This is because, in marine settings, the early-diagenetic pore water REE inventories, and thus Nd isotope signals, are typically dominated by reduction of marine-derived, authigenic Fe-Mn oxides and sedimentary organic matter, and thus resemble the local seawater signature (Martin and Haley, 2000; Gutjahr et al., 2007; Molina-Kescher et al., 2014). As a result, as long as no exotic Nd is locally introduced by seepage of deep-seated fluids (cf., Jakubowicz et al., 2019), the offset between deep seawater and shallow-burial pore water values is typically insignificant and does not exceed 1–1.5 ε_{Nd} units even for profiles exceptionally rich in volcanic ash dispersed within the sediment (Abbott et al., 2015). Consequently, fish teeth provide a valuable archive of secular changes in the Nd isotope signature of seawater in marine basins.

Here, we present a late Oligocene to early Pleistocene record of oceanographic conditions in the south-eastern Pacific Ocean based on the Nd isotope composition of shark teeth enameloid from the Pisco and Sacaco basins in south-central Peru.

2. Material and methods

The Pisco and Sacaco basins (Fig. 2) are located at 13–16°S, contain Eocene to Pleistocene shallow marine sedimentary sequences deposited at depths not deeper than ~150 m, and are renowned for their diverse marine mammal fauna (Bosio et al., 2021; Collareta et al., 2021; Ochoa et al., 2021). For our analysis, teeth of a genus of coastal shark (*Carcharhinus*) without inter-oceanic migratory behavior (Schultz et al., 2008; Benavides et al., 2011) were used to ensure that the isotope signal reflects local water masses. Most teeth belong to *Carcharhinus brachyurus*, with additional specimens of *C. leucas* and *C.* aff. *macloti*, and a few that could not be assigned with confidence to any of these species, but belong to *Carcharhinus*. The material was partly collected during a field trip in 2018 and supplemented by specimens housed in the Departamento de Paleontología de Vertebrados del Museo de Historia Natural, Universidad Nacional Mayor de San Marcos de Lima (MUSM) in Peru (Table 1).

The shark-tooth fluorapatite samples (5–18 mg) were spiked with ^{150}Nd–^{149}Sm enriched tracer and dissolved in concentrated HNO_3. Separation of Nd and Sm was performed on 2 ml columns packed with EICHROM Ln resin. Both elements were eluted with ultrapure HCl, 0.25 N and 0.75 N, respectively. Nd and Sm (loaded as phosphate) were measured on Re in a double filament configuration. The Nd–Sm isotope analyses were performed at the Isotope Laboratory of the Adam Mickiewicz University, Poznań (Poland), on a Finnigan MAT 261 multi-collector thermal ionization mass spectrometer running in a static (Sm) and dynamic (Nd) mode. The AMES standard yielded $^{143}Nd/^{144}Nd$ = 0.512128 ± 10 (2σ; n = 15). The $^{143}Nd/^{144}Nd$ ratios were normalized to $^{146}Nd/^{144}Nd$ = 0.7219 and Sm isotope ratios to $^{147}Sm/^{152}Sm$ = 0.56081. Total procedure blanks were < 40 pg for both Nd and Sm. Nd isotope data are reported in the standard ε notation calculated using $^{143}Nd/^{144}Nd$ = 0.512638 and $^{147}Sm/^{144}Nd$ = 0.1967 for present-day CHUR (Jacobsen and Wasserburg, 1980) (see Table 2).

3. Results and interpretation

Overview. Most measured late Oligocene to Pleistocene shark teeth ε_{Nd} values from the Pisco and Sacaco basins range from −4.3 to −0.7, with a remarkable excursion at around 8–7 million years ago (Ma), when ε_{Nd} values dropped to −9.2 (Fig. 3A; Table 2). The Pisco/Sacaco ε_{Nd} curve shows the same overall trend towards more radiogenic values as the deep equatorial Pacific ε_{Nd} curve, though with an offset of +2 ε_{Nd} units from 25 to 9 Ma. This offset disappears after the late Miocene negative excursion. From about 2.5 Ma onward, the Pisco/Sacaco ε_{Nd} curve shows the same trend toward less radiogenic values as the deep equatorial Pacific ε_{Nd} curve (Fig. 3A).

Weathering inputs. Interpreting these data requires careful consideration of potential Nd sources, which include both the coastal water masses and local input. Ehlert et al. (2013) proposed that ε_{Nd} values found in Mn–Fe coatings of particles and benthic foraminifers along the Peruvian coast follow the local water and detritus values, and concluded that the coastal ε_{Nd} signatures

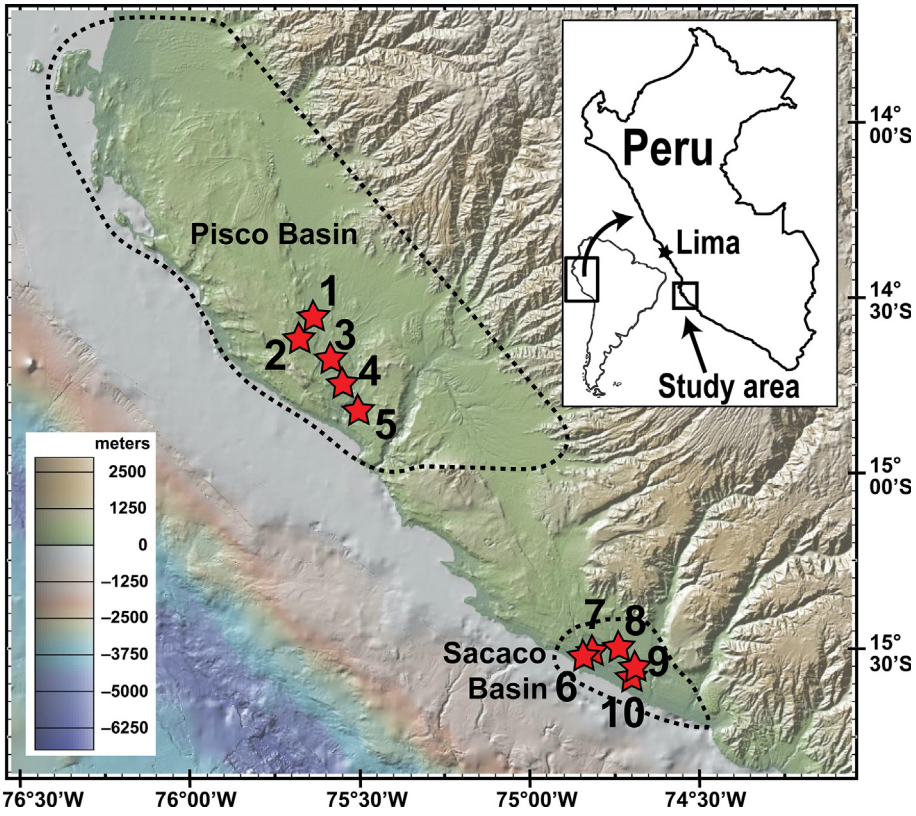

Fig. 2. Sample locations in the Pisco and Sacaco basins in south-central Peru. Numbers refer to locality numbers in Table 1. Modified from www.geomapapp.org (Ryan et al., 2009).

Table 1
Samples and sampling sites used in this study. MUSM = Museo de Historia Natural, Universidad Nacional Mayor San Marcos, Departamento de Paleontología de Vertebrados, Lima, Peru. Stratigraphy and ages from Ochoa et al. (2021), Di Celma et al. (2017), DeVries et al. (2021), and DeVries and Jud (2018).

Sample no. [MUSM]	Locality (number on figures)	Formation	Age	Coordinates	Reference
3773–3775	Lomas Blancas de Caracoles (10)	Pongo	early Pleistocene	15°30′21.26″S, 74°44′43.10″W	Ochoa et al. 2021
3770	Quebrada Caracoles (9)	Caracoles	earliest Pleistocene	15°30.206′S, 74°44,541′W	Ochoa et al. 2021
3783	Sacaco Este (8)	Pisco	latest Miocene	15°35.176′S, 76°40.244′W	Ochoa et al. 2021
3231	Aguada de Lomas (7)	Pisco	late Miocene	15°30′43.84″S, 74°48′50.39″W	Ochoa et al. 2021
3785	Lomas (6)	Pisco	late Miocene (stratigraphically below Aguada de Lomas)	15° 32′ 43″S, 74° 50′ 22″W	Ochoa et al. 2021
3776, 3777	Cerro La Bruja (5)	Pisco	late Miocene, c. 9 Ma	14°31′27″S, 75°40′13″W	Di Celma et al. 2017
3778–3780	Gramadal (4)	Pisco	late middle Miocene	14°44′43″S, 75°32′58″W	DeVries et al. 2021
3781, 3782	Ullujaya (3)	Chilcatay	early Miocene, 19 Ma	14°35′2.70″S, 75°38′24.80″W	DeVries and Jud 2018
3739–3743, 3759, 3760	Samaca East (2)	Chilcatay	early Miocene	14°37.396′S, 75°38.749′W	DeVries and Jud 2018
3746–3748, 3754, 3755	Samaca West (1)	Chilcatay	late Oligocene	14°41.819′S, 75°35.830′W	DeVries and Jud 2018

broadly reflect local weathering inputs and hinterland geology. The main rocks exposed in the drainage area of the Pisco and Sacaco basins include Precambrian basement (with ε_{Nd} values of ~−5 to −4), Paleozoic crust (ε_{Nd} ~−1.5 to −1), Mesozoic volcanics (ε_{Nd} ~1 to 3), the Cretaceous Coastal Batholith (ε_{Nd} ~0 to 3) and Cenozoic volcanics (ε_{Nd} ~ −5 to +2) (Soler and Rotach-Toulhoat, 1990; Vatin-Pérignon et al., 1992; Martínez Ardila et al., 2019). A recent provenance analysis showed that material of the most Miocene to Pleistocene clastics in the Pisco/Sacaco basin is derived from Mesozoic and Cenozoic sources, though until 6 Ma there was also input from a somewhat enigmatic late Neoproterozoic source (Ochoa et al., 2022).

Weathering inputs from the whole range of hinterland rocks could potentially have produced most of the values seen in the Pisco/Sacaco shark teeth, but not the Mesozoic and Cenozoic sources alone. None of the known hinterland rocks could have produced values as low as those of the late Miocene negative excursion, at least assuming that the unknown Neoproterozoic source has ε_{Nd} values similar to those of the known Precambrian basement. The history of Andean uplift is still under debate, but most studies agree that the Western Cordillera reached a near-modern elevation well before or during the mid-Miocene, with relatively little change afterward, and the more easterly located Eastern Cordillera and Altiplano reached their present-day elevation during

Table 2
Results of the Nd isotope analysis. MUSM = Museo de Historia Natural, Universidad Nacional Mayor San Marcos, Departamento de Paleontología de Vertebrados, Lima, Peru. * Types of shark tooth fluorapatite material: e – enameloid, d – dentine.

Specimen no. [MUSM]	Locality number	Material type	Weight [mg]	Sm [ppm]	Nd [ppm]	147Sm/144Nd	143Nd/144Nd (t)	eNd (t)	Species (C.)	Age
3773	10	e	9.03	2.52	13.3	0,1144	0,512499 ± 15	−2.7	*C. brachyurus*	early Pleistocene
3774	10	e	17.89	5.6	33.15	0,1021	0,512555 ± 13	−1.6	*C. brachyurus*	early Pleistocene
3775	10	e	15.02	7.73	43.34	0,1078	0,512549 ± 10	−1.7	*C.* sp.	early Pleistocene
3770	9	e + d	16.5	1.48	7.19	0,124	0,512586 ± 14	−1	*C.* sp.	earliest Pleistocene
3783	8	e + d	13.59	16.51	84.17	0,1186	0,512505 ± 10	−2.4	*C. leucas*	latest Miocene
3231	7	e + d	5.98	56.68	276.64	0,1239	0,512160 ± 8	−9.1	*C.* sp.	late Miocene
3785	6	e + d	15.16	12	57.09	0,1271	0,512159 ± 15	−9.2	*C. brachyurus*	late Miocene
3776	5	e	10.63	58.16	292.26	0,1203	0,512588 ± 10	−0.7	*C. brachyurus*	late Miocene, c. 9 Ma
3777	5	e	10.09	34	155.23	0,1324	0,512588 ± 10	−0.8	*C. brachyurus*	late Miocene, c. 9 Ma
3778	4	e	10.05	24.54	136.32	0,1088	0,512518 ± 10	−2	*C. brachyurus*	late middle Miocene
3779	4	e	3.38	31.15	168.3	0,1119	0,512511 ± 7	−2.2	*C.* sp.	late middle Miocene
3780	4	e	11	32.94	180.48	0,1103	0,512523 ± 9	−1.9	*C.* sp.	late middle Miocene
3781	3	e	9.44	10.26	51.36	0,1208	0,512529 ± 10	−1.6	*C. brachyurus*	early Miocene, 19 Ma
3782	3	e + d	5.94	31.03	165.64	0,1132	0,512461 ± 10	−2.9	*C.* sp.	early Miocene, 19 Ma
3739	2	e	9.34	21.66	119.05	0,11	0,512390 ± 10	−4.3	*C. brachyurus*	early Miocene
3740	2	e	19.7	21.01	119.62	0,1062	0,512428 ± 10	−3.5	*C. brachyurus*	early Miocene
3741	2	e	8.99	24.88	150.76	0,0998	0,512434 ± 11	−3.4	*C.* aff. *macloti*	early Miocene
3742	2	e + d	10.52	60.1	337.62	0,1077	0,512461 ± 10	−2.9	*C.* sp.	early Miocene
3743	2	e + d	11.9	13.5	77.8	0,1048	0,512418 ± 15	−3.7	*C.* sp.	early Miocene
3759	2	e	10.43	11.82	62.71	0,114	0,512490 ± 13	−2.3	*C. brachyurus*	early Miocene
3760	2	e	9.84	6.11	37.99	0,0973	0,512493 ± 9	−2.3	*C. brachyurus*	early Miocene
3746	1	e	8.49	19.29	106.47	0,1096	0,512493 ± 9	−2.2	*C. brachyurus*	late Oligocene
3747	1	e + d	10.75	77.14	295.13	0,158	0,512503 ± 7	−2	*C.* sp.	late Oligocene
3748	1	e	11.99	12.64	64.98	0,1176	0,512514 ± 10	−1.8	*C.* sp.	late Oligocene
3754	1	e	10.88	21.64	117.75	0,1111	0,512461 ± 10	−2.8	*C.* sp.	late Oligocene
3755	1	e	14.65	54.04	246.92	0,1323	0,512448 ± 7	−3.1	*C. brachyurus*	late Oligocene

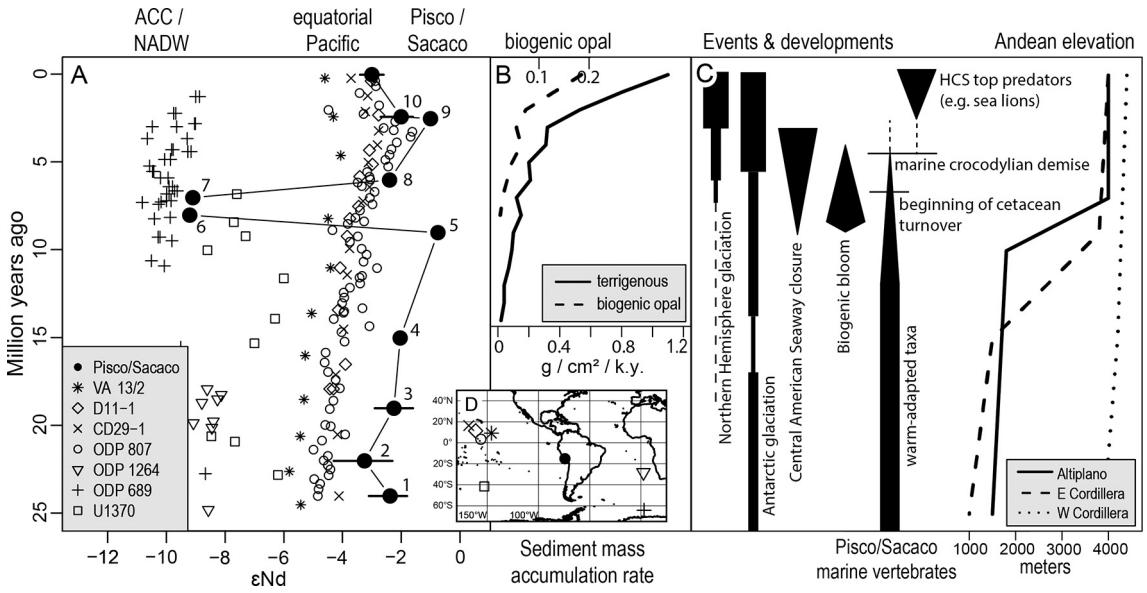

Fig. 3. A. Late Oligocene to Pleistocene shark teeth ε_{Nd} values from the Pisco and Sacaco basins, Peru (filled circles); horizontal bars indicate ranges of values pooled by locality; numbers indicate sampling sites given in Fig. 2 and Table 1; present-day values for the Pisco/Sacaco basins from stations 30 and 78 of Grasse et al. (2012), at 3 and 2 m water depth, respectively. For comparison, we include ε_{Nd} values from the deep equatorial Pacific [data for sites VA13/2, D11-1 and CD29-1 from Ling et al. (1997); for ODP 807 from Le Houedec et al. (2016)], the Antarctic Circumpolar Current [data from ODP site 689 for 25–17 Ma, from Scher and Martin (2004), and for site U1370 from McKinley et al. (2019)] and North Atlantic Deep Water (NADW) from ODP hole 1264 on the Walvis Ridge in the South Atlantic Ocean, the nearest water mass feeding into the Pacific part of the ACC for which Neogene ε_{Nd} data are available [data from Thomas and Via (2007)]. Locations are shown in inset D. **B.** Sediment mass accumulation rates (MAR) offshore Peru; terrigenous MAR as a proxy for dust flux, biogenic opal MAR as a proxy for paleoproductivity; note different scales for each (data from Tiedemann and Mix, 2007, fig. F9). **C.** Related local and global trends. Events and developments from Steinthorsdottir et al. (2021); Pisco/Sacaco marine vertebrate fauna from Collareta et al. (2021) and Ochoa et al. (2021); Andean elevations from Boschman (2021).

the mid to late Miocene (Fig. 3C; cf. Gregory-Wodzicki, 2000; Thouret et al., 2007; Prudhomme et al., 2019; Sundell et al., 2019; Boschman, 2021). Furthermore, the south-central Peruvian margin has, on average, been very dry since the Miocene (Hartley et al., 2005; Garreaud et al., 2010; Amidon et al., 2017). Therefore, large changes in the input of weathering products into the Pisco and Sacaco basins may not be expected.

A significant part of the upwelling waters along the Peruvian coast originate from the southward-flowing Peru-Chile Undercurrent, which in turn is fed by the Equatorial Undercurrent (Fig. 1; Montecino and Lange, 2009). The ε_{Nd} signature of this current is around −3 to −1 (Grasse et al., 2012; Haley et al., 2021) and thus not unlike that of the Pisco/Sacaco shark teeth. Interestingly, the ε_{Nd} values of extant foraminiferans and Mn–Fe coatings published by Ehlert et al. (2013) from the area with the strongest permanent upwelling along the Peruvian coast (5-15°S, cf. Montecino and Lange, 2009) are remarkably uniform with a mean around −1, consistent with the ε_{Nd} signature of the PCUC and EUC (Grasse et al., 2012; Haley et al., 2021), which nearly reaches the surface in this area (Chaigneau et al., 2013). Thus, with (i) major changes in the input of weathering products and associated changes in the ε_{Nd} signature of the Pisco and Sacaco basin sediments since the late Oligocene being unlikely, and (ii) proxies for the present-day ε_{Nd} signature of the waters along the central Peruvian coast (foraminiferans and Mn–Fe coatings) showing values of the upwelling, underlying water masses, we assume that the longer-term trends seen in our shark teeth ε_{Nd} data should provide insights into the general oceanographic conditions along the south-central Peruvian coast.

The general resemblance of the ε_{Nd} curves of the Pisco/Sacaco basins and deep equatorial Pacific Ocean (except for the late Miocene negative excursion and the +2 offset before 9 Ma) is striking. Although the PCUC and EUC are not fed by equatorial Pacific bottom waters (most EUC waters originate in the Solomon basin just east of Papua New Guinea, cf. Tsuchiya et al., 1989; Grenier et al., 2011), we interpret this resemblance as further indication that the Pisco/Sacaco shark ε_{Nd} values reflect an open marine signal, rather than hinterland weathering. Furthermore, we consider it unlikely that changes in weathering in the hinterland should coincidentally have reproduced the ε_{Nd} trend of the deep equatorial Pacific Ocean. Rather, we interpret the Pisco/Sacaco shark ε_{Nd} data as evidence that upwelling occurred along the Peruvian coast at least since the late Oligocene, consistent with earlier studies (von Huene et al., 1987; Marty et al., 1988; Lagabrielle et al., 2009; Armijo et al., 2015; DeVries et al., 2017).

The +2 offset before 9 Ma. The offset of +2 ε_{Nd} units before 9 Ma in the Pisco/Sacaco ε_{Nd} record compared to the equatorial Pacific record and its subsequent disappearance (Fig. 3A) suggests changes in the origin, proportions, and/or intensity of the upwelling waters. The source area of the EUC, the Solomon Basin, is surrounded largely by young volcanic rocks, and the present-day NE directed South Solomon Arc volcanism started about 6 Ma (Smith, 1982; Petterson et al., 1999). Thus increased input from this source, if any, should have resulted in higher rather than the observed lower ε_{Nd} values after 6 Ma.

Strengthened or even permanent El Niño conditions have been discussed for the Pliocene and Miocene (Fedorov et al., 2006; Von Der Heydt and Dijkstra, 2011). Such conditions could have subdued upwelling along the Peruvian coast and could potentially account for the higher ε_{Nd} values in the Miocene Pisco record. However, the evidence for permanent El Niño conditions is controversial (Steinthorsdottir et al., 2021) and other studies instead indicate present-day El Niño variability for the Mio-Pliocene (Batenburg et al., 2011; Watanabe et al., 2011; Okamura et al., 2013; Pérez-Rivarés et al., 2019). Thus, the 'permanent El Niño' is here not considered further to explain the +2 ε_{Nd} units offset in the Pisco/Sacaco data, though it may not be completely ruled out.

The disappearance of the +2 offset at 8–6 Ma broadly coincides with the time when the Altiplano reached its present-day elevation and with increased glaciation in Antarctica (Fig. 3). Andean uplift

has been associated with increased upwelling along the Peruvian coast, because it enhances northward along-shore wind strength (Sepulchre et al., 2009). Likewise, an expanding West Antarctic ice sheet would steepen the latitudinal temperature gradient and increase counter-clockwise circulation in the southern Pacific Ocean (Holbourn et al., 2018; Steinthorsdottir et al., 2021). This in turn could have enhanced the transport of Antarctic waters towards the Pacific margin of South America, including Sub-Antarctic Mode Water that feeds into the upwelling waters along the Peruvian coast. Enhanced input of SAMW with its negative ε_{Nd} signature into the upwelling water mass could thus have eliminated the +2 offset at 6 Ma in the Pisco/Sacaco record. Another potential explanation for the disappearance of the +2 offset is the exhaustion of an enigmatic Neoproterozoic source rock in the hinterland at this time (cf., Ochoa et al., 2022) that could have contributed unradiogenic Nd to the Pisco/Sacaco signal. But because the disappearance of the +2 offset coincides with a gradual change in the Pisco/Sacaco marine vertebrate record toward more cold-adapted faunas (Collareta et al., 2021; Ochoa et al., 2021), we consider increased upwelling of colder water the more likely scenario.

The late Miocene negative excursion. The most remarkable deviation from the general 'equatorial Pacific' trend occurred in the late Miocene about 8–7 Ma, when ε_{Nd} values dropped to –9.2. These values are lower than those of any of the rocks in the hinterland – including the Paleozoic basement (Ehlert et al., 2013; Martínez Ardila et al., 2019; Robinson et al., 2021). Also dust input from the Andes to the equatorial eastern Pacific does not show a marked increase at this time (Fig. 3B; cf. Tiedemann and Mix, 2007). Thus, changes in terrestrial input from hinterland weathering are an unlikely driver of this negative excursion. The values are also well below those of coeval Pacific deep water (Fig. 3A; see also McKinley et al., 2019), Pacific surface waters and shallow marine sediments, and of rocks in the hinterlands of the Pacific continental margins (Robinson et al., 2021), thus indicating an input of oceanic water masses from elsewhere.

Potential sources with such low ε_{Nd} values are a direct influx of Antarctic water or an influx from the Atlantic Ocean via the Central American Seaway (Lacan et al., 2012). Flow through the Central American Seaway is typically considered to run from the Pacific into the Atlantic Ocean, rather than vice versa (Iturralde-Vinent and MacPhee, 1999; Heydt and Dijkstra, 2005), and with progressive shallowing of this seaway during the late Miocene, the flux should have decreased, rather than increased. Furthermore, Caribbean seawater ε_{Nd} values reconstructed based on fish teeth and debris of this age are only as low as –7.3 (Newkirk and Martin, 2009), which is too high to explain the Pisco/Sacaco basin values of –9.2. However, oceanographic modeling of the Central American Seaway indicates that at a certain depth of the seaway (~50 m), wind-driven surface waters would flow westward from the Atlantic into the Pacific Ocean (Sepulchre et al., 2014), from where they could potentially reach the Peruvian coast. Interestingly, this would be a short-lived event due to the continued shallowing and ultimate closure of the seaway, thereby providing a mechanism to end the negative excursion.

The other source of water masses with ε_{Nd} values negative enough to explain our data is Antarctic water (Basak et al., 2015; McKinley et al., 2019). This explanation could involve either a direct influx of surface water (i.e., a proto-Humboldt current) or an increased contribution of deeper Antarctic waters (AAIW/SAMW) to the upwelling water. Enhanced input of surface water would be possible given increased atmospheric and oceanic circulation (see discussion of mechanisms below) as it would result in increased export of northern ACC water into the Humboldt Current System (Lamya et al., 2015).

The main area of AAIW and SAMW formation today lies northwest of the Antarctic Peninsula, from where it is transported NW-ward into the South Pacific (Hartin et al., 2011; Bostock et al., 2013). Among these water masses, SAMW is known to feed into the upwelling water along the Peruvian coast (Montes et al., 2010; Toggweiler et al., 2019). Although the northern limit of the AAIW near the South American coast was considered to lie between 18 and 22°S today (Bostock et al., 2013), Grasse et al. (2012) reported potential AAIW from as far north as 9°S, albeit only at depth of c. 800 m and thus not reaching the surface mixing zone. Furthermore, modeling of Nd isotope distributions indicates that AAIW flows northward into the Pacific Ocean at depths between 500 m and 1000 m and nearly reaches the equator (Arsouze et al., 2007, fig. 5a).

There are two potential mechanisms and triggers that might have increased upwelling and allowed AAIW to reach surface waters: a coeval pulse of uplift of the Altiplano of the Andes (Kar et al., 2016; Schildgen and Hoke, 2018; Boschman, 2021) resulting in increased wind stress along the Peruvian coast (cf. Montecino and Lange, 2009; Sepulchre et al., 2009), and growth of the Antarctic ice sheet, resulting in a steeper equator to pole temperature gradient (Holbourn et al., 2018; Steinthorsdottir et al., 2021). Climate modeling suggests that a climate warmer than today (as expected for the late Miocene) would increase the thermal stratification of the water column and decrease the depth of the upwelling source waters (Oerder et al., 2015; Wang et al., 2015), making it less likely for AAIW to reach surface waters. However, an analysis of sediment distribution on the Nazca Drift System offshore Peru showed a period of intense northward bottom current c. 7.7 to 9.4 Ma (Calvès et al., 2022), indicating an enhanced Antarctic Circumpolar Current and associated northward export of Antarctic waters coincident with the late Miocene negative ε_{Nd} excursion in the Pisco and Sacaco basins. Also consistent with ~~an~~ increased input of deeper, nutrient-rich, Antarctic waters to the upwelling water is the increased deposition of diatomite mud in the Pisco/Sacaco basin from around 8 Ma (Di Celma et al., 2017).

The late Miocene negative excursion of the Pisco/Sacaco shark ε_{Nd} record shows a remarkable coincidence with a global, late Miocene to early Pliocene biogenic bloom and associated high opal and $CaCO_3$ deposition (Peterson et al., 1992; Tiedemann and Mix, 2007). The timing and duration of this biogenic bloom varied somewhat between ocean basins (Karatsolis et al., 2022); in the Pacific Ocean, it was strongest between about 8 and 6.4 Ma (Suto et al., 2012; Karatsolis et al., 2022), consistent with the negative ε_{Nd} excursion in the Pisco/Sacaco basin. The biogenic bloom has been attributed to various causes, including ocean fertilization by dust input due to increased aridity in central Asia and South America (Suto et al., 2012), the closure of the Central American Seaway (Lyle and Baldauf, 2015), and the growth of the Antarctic ice sheet, resulting in the strengthening of trade winds and associated increased upwelling (Holbourn et al., 2018). Our data and interpretation of the late Miocene negative ε_{Nd} excursion in the Pisco/Sacaco basin would support the hypothesis of increased upwelling during this time (Holbourn et al., 2018; Steinthorsdottir et al., 2021). Furthermore, increased input of AAIW/SAMW to the upwelling waters along the Pacific coast of South America could have been an important contributor to the biogenic bloom.

The HCS ecosystem. In the Pisco and Sacaco basins, the late Miocene negative ε_{Nd} excursion was associated with a decrease in the diversity of cetaceans (baleen and toothed whales) that is mirrored in a global decrease in cetacean diversity (Marx and Uhen, 2010; Villafaña and Rivadeneira, 2014). The negative excursion and the disappearance of the +2 offset between the Pisco/Sacaco and the equatorial Pacific ε_{Nd} record coincide with a gradual change in the Pisco/Sacaco marine mammal record toward more cold-adapted faunas (Fig. 3; Collareta et al., 2021; Ochoa et al., 2021). After a 14-million-year record of two marine crocodylian species in the Pisco/Sacaco basins, their disappearance from coastal

environments at about the earliest Pliocene (Salas-Gismondi et al., 2022) provides further evidence for our hypothesis of an increased contribution of Antarctic waters to the upwelling waters along the Peruvian coast.

The present-day Humboldt Current upwelling ecosystem has a characteristic structure in which a few species of extremely abundant, plankton-feeding 'forage fishes', such as sardines and anchovy, link the planktonic primary production to the generalized predators (Alheit and Niquen, 2004). The suggested increased contribution of Antarctic waters into the Pisco/Sacaco basins since 9 Ma – carrying along abundant silica – might have facilitated the onset of this present-day food web structure. This is suggested by the stomach content of a diversity of large predatory vertebrates (baleen whales, sharks, ziphiid odontocetes) from the upper part of the Pisco Formation (8–7 Ma), which consisted mainly of the same sardine fish, despite their different feeding anatomies (Collareta et al., 2021). Thus, increased primary productivity induced by the suggested input of silica-rich Antarctic water could have catalyzed the onset of the forage fish-based food web seen in the Humboldt Current upwelling ecosystem today.

Also remarkable is that the abrupt shift in the Sacaco basin shark ε_{Nd} values toward the less radiogenic present-day values at 2.5 Ma (Fig. 3) coincides with the first appearance of taxa related to present-day top predators (sea lions, bottlenose dolphins) of the Humboldt Current upwelling ecosystem (Ochoa et al., 2021) and with a massive increase in bioproductivity offshore northwestern South America, as indicated by increased biogenic opal deposition (Fig. 3B, cf. Tiedemann and Mix, 2007). The coeval shift toward less radiogenic ε_{Nd} values in the deep tropical Pacific Ocean was interpreted as an increased NADW component via the ACC (Ling et al., 1997). Thus, increased Northern Hemisphere glaciation (Fig. 3C, cf. Zachos et al., 2001; Steinthorsdottir et al., 2021) resulting in enhanced input of cold, nutrient-rich NADW into the ACC and from there toward the South America Pacific coast, might ultimately have shaped the modern Humboldt Current ecosystem.

4. Conclusions

The late Oligocene through Pleistocene ε_{Nd} signatures of shark tooth enameloid from the Pisco and Sacaco basins in southern Peru provide new insights into the origin of the water masses bathing these basins. Overall our data are consistent with upwelling since the late Oligocene. The upwelling waters today are a mix of equatorial subsurface waters and deeper Antarctic waters (SAMW). The Pisco/Sacaco ε_{Nd} data indicate that the contribution of southern-sourced waters was lower than today until the late Miocene, and the change to approximately present-day mixing proportions was coincident with increased Antarctic glaciation and with the Andes reaching their present-day elevation. Both of these factors likely enhanced the counter-clockwise circulation in the South Pacific Ocean, thereby increasing the contribution of deeper Antarctic waters to the upwelling waters along the Peruvian coast.

A remarkable negative excursion of ε_{Nd} values occurred about 8–7 Ma, indicating an even stronger, though short-lived, influx of Antarctic waters. This event coincides with a late Miocene biogenic bloom recorded across the Pacific Ocean. We propose that the northward spread of Antarctic Intermediate Waters likely was an important contributor to this biogenic bloom. The general trend in the Pisco/Sacaco ε_{Nd} data toward more radiogenic values was reversed at about 2.5 Ma, coincident with extensive glaciation in the Northern Hemisphere, resulting in increased transport of cold North Atlantic Deep Water with a very unradiogenic ε_{Nd} signature, into the Southern Ocean. These Northern Hemisphere water masses may ultimately have established the present-day forage fish-based food web of the Humboldt Current upwelling ecosystem.

CRediT authorship contribution statement

Steffen Kiel: Conceptualization, Investigation, Writing – original draft, Visualization. **Michal Jakubowicz:** Conceptualization, Investigation, Writing – original draft. **Alí Altamirano:** Investigation, Resources. **Zdzislaw Belka:** Investigation. **Jolanta Dopieralska:** Investigation. **Mario Urbina:** Resources. **Rodolfo Salas-Gismondi:** Resources, Writing – review & editing.

Declaration of Competing Interest

The authors declare that they have no known competing financial interests or personal relationships that could have appeared to influence the work reported in this paper.

Acknowledgments

We thank Helen Coxall and Agatha de Boer (University of Stockholm, Sweden), and Matt Huber (Purdue University, West Lafay ette, USA) for discussions on paleoceanography. Alberto Collareta (Pisa), Gérôme Calvès (Toulouse), and three anonymous reviewers are thanked for their constructive criticism that helped improving the manuscript. Financial support was provided by the Bolin Centre for Climate Research (Stockholm, Sweden) to SK, and by Prociencia/Concytec research grants (E38-2019-02-Fondecyt-BM, 104-2018-Fondecyt, and 149-2018-Fondecyt-BM-IADT-AV) to RS-G.

References

Abbott, A.N., Haley, B.A., McManus, J., 2015. Bottoms up: Sedimentary control of the deep North Pacific Ocean's εNd signature. Geology 43, 1035–1038.
Alheit, J., Niquen, M., 2004. Regime shifts in the Humboldt Current ecosystem. Prog. Oceanogr. 60, 201–222.
Amidon, W.H., Fisher, G.B., Burbank, D.W., Ciccioli, P.L., Alonso, R.N., Gorin, A.L., Silverhart, P.H., Kylander-Clark, A.R.C., Christoffersen, M.S., 2017. Mio-Pliocene aridity in the south-central Andes associated with Southern Hemisphere cold periods. Proc. Natl. Acad. Sci. 114, 6474–6479.
Armijo, R., Lacassin, R., Coudurier-Curveur, A., Carrizo, D., 2015. Coupled tectonic evolution of Andean orogeny and global climate. Earth Sci. Rev. 143, 1–35.
Arsouze, T., Dutay, J.-C., Lacan, F., Jeandel, C., 2007. Modeling the neodymium isotopic composition with a global ocean circulation model. Chem. Geol. 239, 165–177.
Basak, C., Pahnke, K., Frank, M., Lamy, F., Gersonde, R., 2015. Neodymium isotopic characterization of Ross Sea Bottom Water and its advection through the southern South Pacific. Earth Planet. Sci. Lett. 419, 211–221.
Batenburg, S.J., Reichart, G.-J., Jilbert, T., Janse, M., Wesselingh, F.P., Renema, W., 2011. Interannual climate variability in the Miocene: High resolution trace element and stable isotope ratios in giant clams. Palaeogeogr. Palaeoclimatol. Palaeoecol. 306, 75–81.
Benavides, M.T., Feldheim, K.A., Duffy, C.A., Wintner, S., Braccini, J.M., Boomer, J., Huveneers, C., Rogers, P., Mangel, J.C., Alfaro-Shigueto, J., Cartamil, D.P., Chapman, D.D., 2011. Phylogeography of the copper shark (*Carcharhinus brachyurus*) in the southern hemisphere: implications for the conservation of a coastal apex predator. Mar. Freshw. Res. 62, 861–869.
Boschman, L.M., 2021. Andean mountain building since the Late Cretaceous: A paleoelevation reconstruction. Earth Sci. Rev. 220, 103640.
Bosio, G., Malinverno, E., Collareta, A., Celma, C.D., Gioncada, A., Parente, M., Berra, F., Marx, F.G., Vertino, A., Urbina, M., Bianucci, G., 2020. Strontium Isotope Stratigraphy and the thermophilic fossil fauna from the middle Miocene of the East Pisco Basin (Peru). J. S. Am. Earth Sci. 97, 102399.
Bosio, G., Collareta, A., Celma, C.D., Lambert, O., Marx, F.G., Muizon, C.D., Gioncada, A., Gariboldi, K., Malinverno, E., Malca, R.V., Urbina, M., Bianucci, G., 2021. Taphonomy of marine vertebrates of the Pisco Formation (Miocene, Peru): Insights into the origin of an outstanding Fossil-Lagerstätte. PLoS ONE 16.
Bostock, H.C., Sutton, P.J., Williams, M.J.M., Opdyke, B.N., 2013. Reviewing the circulation and mixing of Antarctic Intermediate Water in the South Pacific using evidence from geochemical tracers and Argo float trajectories. Deep-Sea Res. II 73, 84–98.

Calvès, G., Mix, A., Giosan, L., Clift, P., Brusset, S., Baby, P., Vega, M., 2022. The Nazca Drift System – palaeoceanographic significance of a giant sleeping on the SE Pacific Ocean floor. Geol. Mag. 159, 322–336.
Chaigneau, A., Dominguez, N., Eldin, G., Vasquez, L., Flores, R., Grados, C., Echevin, V., 2013. Near-coastal circulation in the Northern Humboldt Current System from shipboard ADCP data. J. Geophys. Res. Oceans 118, 5251–5266.
Chavez, F.P., Bertrand, A., Guevara-Carrasco, R., Jorge Csirke, P.S., 2008. The northern Humboldt Current System: Brief history, present status and a view towards the future. Prog. Oceanogr. 79, 95–105.
Collareta, A., Lambert, O., Marx, F.G., de Muizon, C., Varas-Malca, R.M., Landini, W., Bosio, G., Malinverno, E., Gariboldi, K., Gioncada, A., Urbina, M., Bianucci, G., 2021. Vertebrate palaeoecology of the Pisco Formation (Miocene, Peru): Glimpses into the ancient Humboldt Current Ecosystem. J. Marine Sci. Eng. 9, 1188.
DeVries, T.J., Barron, J., Urbina, M., Ochoa, D., Esperante, R., Snee, L.W., 2021. The Miocene stratigraphy of the Laberinto area (Río Ica Valley) and its bearing on the geological history of the East Pisco Basin (south-central Peru). J. S. Am. Earth Sci. 111, 103458.
DeVries, T.J., Jud, N.A., 2018. Lithofacies Patterns and Paleogeography of the Miocene Chilcatay and lower Pisco Depositional Sequences (East Pisco Basin, Peru). Boletín de la Sociedad Geológica del Perú Volumen Jubilar N° 8, 124–167.
DeVries, T.J., Urbina, M., Jud, N.A., 2017. The Eocene-Oligocene Otuma depositional sequence (East Pisco Basin, Peru): Paleogeographic and paleoceanographic implications of new data. Boletín de la Sociedad Geológica del Perú 112, 14–38.
Di Celma, C., Malinverno, E., Bosio, G., Collareta, A., Gariboldi, K., Gioncada, A., Molli, G., Basso, D., Varas-Malca, R.M., Pierantoni, P.P., Villa, I.M., Lambert, O., Landini, W., Sarti, G., Cantalamessa, G., Urbina, M., Bianucci, G., 2017. Sequence stratigraphy and paleontology of the Upper Miocene Pisco Formation along the western side of the lower Ica Valley (Ica Desert, Peru). Riv. Ital. Paleontol. Stratigr. 123, 255–273.
Dopieralska, J., Belka, Z., Walczak, A., 2016. Nd isotope composition of conodonts: An accurate proxy of sea-level fluctuations. Gondw. Res. 34, 284–295.
Ehlert, C., Grasse, P., Frank, M., 2013. Changes in silicate utilisation and upwelling intensity off Peru since the Last Glacial Maximum – insights from silicon and neodymium isotopes. Quat. Sci. Rev. 72, 18–35.
Fedorov, A., Dekens, P., McCarthy, M., Ravelo, A., deMenocal, P., Barreiro, M., Philander, S.G., 2006. The Pliocene paradox (mechanisms for a permanent El Niño). Science 312, 1485–1489.
Garreaud, R.D., Molina, A., Farias, M., 2010. Andean uplift, ocean cooling and Atacama hyperaridity: A climate modeling perspective. Earth Planet. Sci. Lett. 292, 39–50.
Grasse, P., L., B., Hathorne, E.C., Böning, P., Pahnke, K., Frank, M., 2017. Short-term variability of dissolved rare earth elements and neodymium isotopes in the entire water column of the Panama Basin. Earth Planet. Sci. Lett. 475, 242–253.
Grasse, P., Stichel, T., Stumpf, R., Stramma, L., Frank, M., 2012. The distribution of neodymium isotopes and concentrations in the Eastern Equatorial Pacific: Water mass advection versus particle exchange. Earth Planet. Sci. Lett. 353–354, 198–207.
Gregory-Wodzicki, K.M., 2000. Uplift history of the Central and Northern Andes: A review. Bull. Geol. Soc. Am. 112, 1091–1105.
Grenier, M., Cravatte, S., Blanke, B., Menkes, C., Koch-Larrouy, A., Durand, F., Melet, A., Jeandel, C., 2011. From the western boundary currents to the Pacific Equatorial Undercurrent: Modeled pathways and water mass evolutions. J. Geophys. Res. 116, C12044.
Gutjahr, M., Frank, M., Stirling, C.H., Klemm, V., van de Flierdt, T., Halliday, A.N., 2007. Reliable extraction of a deepwater trace metal isotope signal from Fe–Mn oxyhydroxide coatings of marine sediments. Chem. Geol. 242, 351–370.
Haley, B.A., Wu, Y., Muratli, J.M., Basak, C., Pena, L.D., Goldstein, S.L., 2021. Rare earth element and neodymium isotopes of the eastern US GEOTRACES Equatorial Pacific Zonal Transect (GP16). Earth Planet. Sci. Lett. 576, 117233.
Hartin, C.A., Fine, R.A., Sloyan, B.M., Talley, L.D., Chereskin, T.K., Happell, J., 2011. Formation rates of Subantarctic mode water and Antarctic intermediate water within the South Pacific. Deep-Sea Res. I 58, 524–534.
Hartley, A.J., Chong, G., Houston, J., Mather, A.E., 2005. 150 million years of climatic stability: evidence from the Atacama Desert, northern Chile. J. Geol. Soc. London 162, 421–424.
Helly, J.J., Levin, L.A., 2004. Global distribution of naturally occurring marine hypoxia on continental margins. Deep-Sea Res. I 51, 1159–1168.
Heydt, A.v.d., Dijkstra, H.A., 2005. Flow reorganizations in the Panama Seaway: A cause for the demise of Miocene corals? Geophys. Res. Lett. 32, L02609.
Holbourn, A.E., Kuhnt, W., Clemens, S.C., Kochhann, K.G.D., Jöhnck, J., Lübbers, J., Andersen, N., 2018. Late Miocene climate cooling and intensification of southeast Asian winter monsoon. Nat. Commun. 9, 1584.
Huck, C.E., van de Flierdt, T., Jiménez-Espejo, F.J., Bohaty, S.M., Röhl, U., Hammond, S. J., 2016. Robustness of fossil fish teeth for seawater neodymiu isotope reconstructions under variable redox conditions in an ancient shallow marine setting. Geochem. Geophys. Geosyst. 17, 679–698.
Iturralde-Vinent, M.A., MacPhee, R.D.E., 1999. Paleogeography of the Caribbean region: implications for Cenozoic biogeography. Bull. Am. Mus. Nat. Hist. 238, 1–95.
Jacobsen, S.B., Wasserburg, G.J., 1980. Sm-Nd isotopic evolution of chondrites. Earth Planet. Sci. Lett. 50, 139–155.
Jakubowicz, M., Dopieralska, J., Kaim, A., Skupien, P., Kiel, S., Belka, Z., 2019. Nd isotope composition of seep carbonates: towards a new approach for constraining subseafloor fluid circulation at hydrocarbon seeps. Chem. Geol. 503, 40–51.
Kar, N., Garzione, C.N., Jaramillo, C., Shanahan, T., Carlotto, V., Pullen, A., Moreno, F., Anderson, V., Moreno, E., Eiler, J., 2016. Rapid regional surface uplift of the northern Altiplano plateau revealed by multiproxy paleoclimate reconstruction. Earth Planet. Sci. Lett. 447, 33–47.
Karatsolis, B.-T., Lougheed, B.C., De Vleeschouwer, D., Henderiks, J., 2022. Abrupt conclusion of the late Miocene-early Pliocene biogenic bloom at 4.6-4.4 Ma. Nat. Commun. 13, 353.
Karstensen, J., Ulloa, O., 2009. Peru-Chile Current System. In: Steele, J.H., Thorpe, S. A., Turekian, K.K. (Eds.), Encyclopedia of Ocean Sciences. second ed. Academic Press, Amsterdam, pp. 385–392.
Kim, S.L., Zeichner, S.S., Colman, A.S., Scher, H.D., Kriwet, J., Mörs, T., Huber, M., 2020. Probing the ecology and climate of the Eocene Southern Ocean with sand tiger sharks *Striatolamia macrota*. Paleoceanogr. Paleoclimatol. 35. e2020PA003997.
Kocsis, L., Trueman, C.N., Palmer, M.R., 2010. Protracted diagenetic alteration of REE contents in fossil bioapatites: Direct evidence from Lu–Hf isotope systematics. Geochim. Cosmochim. Acta 74, 6077–6092.
Lacan, F., Tachikawa, K., Jeandel, C., 2012. Neodymium isotopic composition of the oceans: A compilation of seawater data. Chem. Geol. 300–301, 177–184.
Lagabrielle, Y., Godderis, Y., Donnadieu, Y., Malavieille, J., Suarez, M., 2009. The tectonic history of Drake Passage and its possible impacts on global climate. Earth Planet. Sci. Lett. 279, 197–211.
Lamya, F., Arz, H.W., Kilian, R., Lange, C.B., Lembke-Jene, L., Wengler, M., Kaiser, J., Baeza-Urrea, O., Hall, I.R., Harada, N., Tiedemann, R., 2015. Glacial reduction and millennial-scale variations in Drake Passage throughflow. Proc. Natl. Acad. Sci. 112, 13496–13501.
Le Houedec, S., Meynadier, L., Allègre, C.J., 2016. Seawater Nd isotope variation in the Western Pacific Ocean since 80 Ma (ODP 807, Ontong Java Plateau). Mar. Geol. 380, 138–147.
Ling, H.-F., Burton, K.W., O'Nions, R.K., Kamber, B.S., von Blanckenburg, F., Gibb, A.J., Hein, J.R., 1997. Evolution of Nd and Pb isotopes in Central Pacific seawater from ferromanganese crusts. Earth Planet. Sci. Lett. 146, 1–12.
Lyle, M., Baldauf, J., 2015. Biogenic sediment regimes in the Neogene equatorial Pacific, IODP Site U1338: Burial, production, and diatom community. Palaeogeogr. Palaeoclimatol. Palaeoecol. 433, 106–128.
Martin, E.E., Haley, B.A., 2000. Fossil fish teeth as proxies for seawater Sr and Nd isotopes. Geochim. Cosmochim. Acta 64, 835–847.
Martínez Ardila, A.M., Clausen, B.L., Memeti, V., Paterson, S.R., 2019. Source contamination, crustal assimilation, and magmatic recycling during three flare-up events in the Cretaceous Peruvian Coastal Batholith: An example from the Ica-Pisco plutons. J. S. Am. Earth Sci. 95, 102300.
Marty, R., Dunbar, R., Martin, J.B., Baker, P., 1988. Late Eocene diatomite from the Peruvian coastal desert, coastal upwelling in the eastern Pacific, and Pacific circulation before the terminal Eocene event. Geology 16, 818–822.
Marx, F.G., Uhen, M.D., 2010. Climate, critters, and cetaceans: Cenozoic drivers of the evolution of modern whales. Science 327, 993–996.
McKinley, C.C., Thomas, D.J., LeVay, L.J., Rolewicz, Z., 2019. Nd isotopic structure of the Pacific Ocean 40–10 Ma, and evidence for the reorganization of deep North Pacific Ocean circulation between 36 and 25 Ma. Earth Planet. Sci. Lett. 521, 139–149.
Moiroud, M., Pucéat, E., Donnadieu, Y., Bayon, G., Moriya, K., Deconinck, J.-F., Boyet, M., 2013. Evolution of the neodymium isotopic signature of neritic seawater on a northwestern Pacific margin: new constrains on possible end-members for the composition of deep-water masses in the Late Cretaceous ocean. Chem. Geol. 356, 160–170.
Molina-Kescher, M., Frank, M., Hathorne, E.C., 2014. Nd and Sr isotope compositions of different phases of surface sediments in the South Pacific: Extraction of seawater signatures, boundary exchange, and detrital/dust provenance. Geochem. Geophys. Geosyst. 15, 3502–3520.
Montecino, V., Lange, C.B., 2009. The Humboldt Current System: Ecosystem components and processes, fisheries, and sediment studies. Prog. Oceanogr. 83, 65–79.
Montes, I., Colas, F., Capet, X., Schneider, W., 2010. On the pathways of the equatorial subsurface currents in the eastern equatorial Pacific and their contributions to the Peru-Chile Undercurrent. J. Geophys. Res. Oceans 115, C09003.
Muizon, C.d., Devries, T.J., 1985. Geology and paleontology of late Cenozoic marine deposits in the Sacaco area (Peru). Geol. Rundsch. 74, 547–563.
Newkirk, D.R., Martin, E.E., 2009. Circulation through the Central American Seaway during the Miocene carbonate crash. Geology 37, 87–90.
Ochoa, D., DeVries, T.J., Quispe, K., Barbosa-Espitia, A., Salas-Gismondi, R., Foster, D. A., Gonzales, R., Revillon, S., Berrospi, R., Pairazamán, L., Cardich, J., Perez, A., Romero, P., Urbina, M., Carré, M., 2022. Age and provenance of the Mio-Pleistocene sediments from the Sacaco area, Peruvian continental margin. J. S. Am. Earth Sci. 116, 103799.
Ochoa, D., Salas-Gismondi, R., DeVries, T.J., Baby, P., Muizon, C.d., Altamirano, A., Barbosa-Espitia, A., Foster, D.A., Quispe, K., Cardich, J., Gutiérrez, D., Perez, A., Valqui, J., Urbina, M., Carré, M., 2021. Late Neogene evolution of the Peruvian margin and its ecosystems: a synthesis from the Sacaco record. Int. J. Earth Sci. 110, 995–1025.
Oerder, V., Colas, F., Echevin, V., Codron, F., Tam, J., Belmadani, A., 2015. Peru-Chile upwelling dynamics under climate change. J. Geophys. Res. Oceans 120, 1152–1172.
Okamura, B., O'Dea, A., Taylor, P., Taylor, A., 2013. Evidence of El Niño/La El Niña-Southern Oscillation variability in the Neogene-Pleistocene of Panama revealed by a new bryozoan assemblage-based proxy. Bull. Mar. Sci. 89, 857–876.

Pérez-Rivarés, F.J., Martin-Bello, L., Arenas-Abad, C., 2019. Periodicity in stromatolitic lamination: A potential record of ENSO, NAO, and SUNSPOT in the Miocene lacustrine record of the Ebro Basin, Spain. Sed. Geol. 390, 83–99.
Peterson, L.C., Murray, D.W., Ehrmann, W.U., Hempel, P., 1992. Cenozoic carbonate accumulation and compensation depth changes in the Indian Ocean. Am. Geophys. Union Monograph 70, 311–333.
Petterson, M.G., Babbs, T., Neal, C.R., Mahoney, J.J., Saunders, A.D., Duncan, R.A., Tolia, D., Magu, R., Qopoto, C., Mahoa, H., Natogga, D., 1999. Geological–tectonic framework of Solomon Islands, SW Pacific: crustal accretion and growth within an intra-oceanic setting. Tectonophysics 301, 35–60.
Prudhomme, A., Baby, P., Robert, A., Brichau, S., Cuipa, E., Eude, A., Calderon, Y., O'Sullivan, P., 2019. Western thrusting and uplift in northern Central Andes (western Peruvian margin). In: Horton, B.K., Folguera, A. (Eds.), Andean Tectonics. Elsevier, Amsterdam, pp. 299–331.
Robinson, S., Ivanovic, R., Flierdt, T.v.d., Blanchet, C.L., Tachikawa, K., Martin, E.E., Cook, C.P., Williams, T., Gregoire, L., Plancherel, Y., Jeandel, C., Arsouze, T., 2021. Global continental and marine detrital εNd: An updated compilation for use in understanding marine Nd cycling. Chem. Geol. 567, 120119.
Ryan, W.B.F., S.M. Carbotte, J.C., O'Hara, S., Melkonian, A., Arko, R., Weissel, R.A., Ferrini, V., Goodwillie, A., Nitsche, F., Bonczkowski, J., Zemsky, R., 2009. Global Multi-Resolution Topography (GMRT) synthesis data set. Geochem. Geophys. Geosyst. 10, Q03014.
Salas-Gismondi, R., Ochoa, D., Jouve, S., Romero, P.E., Cardich, J., Perez, A., DeVries, T. J., Baby, P., Urbina, M., Carré, M., 2022. Miocene fossils from the southeastern Pacific shed light on the last radiation of marine crocodylians. Proc. R. Soc. B 289, 20220380.
Salvatteci, R., Gutierrez, D., Sifeddine, A., Ortlieb, L., Druffel, E.R.M., Boussafir, M., Schneider, R., 2016. Centennial to millennial-scale changes in oxygenation and productivity in the Eastern Tropical South Pacific during the last 25,000 years. Quat. Sci. Rev. 161, 102–117.
Scher, H.D., Delaney, M.L., 2010. Breaking the glass ceiling for high resolution Nd isotope records in early Cenozoic paleoceanography. Chem. Geol. 269, 329–338.
Scher, H.D., Martin, E.E., 2004. Circulation in the Southern Ocean during the Paleogene inferred from neodymium isotopes. Earth Planet. Sci. Lett. 228, 391–405.
Scher, H.D., Martin, E.E., 2006. Timing and climatic consequences of the opening of Drake Passage. Science 312, 428–430.
Schildgen, T.R., Hoke, G.D., 2018. The topographic evolution of the central Andes. Elements 14, 231–236.
Schultz, J.K., Feldheim, K.A., Gruber, S.H., Ashley, M.V., McGovern, T.M., Bowen, B.W., 2008. Global phylogeography and seascape genetics of the lemon sharks (genus *Negaprion*). Mol. Ecol. 17, 5336–5348.
Sepulchre, P., Sloan, L.C., Snyder, M., Fiechter, J., 2009. Impacts of Andean uplift on the Humboldt Current system: A climate model sensitivity study. Paleoceanography 24, PA4215.
Sepulchre, P., Arsouze, T., Donnadieu, Y., Dutay, J.-C., Jaramillo, C., Le Bras, J., Martin, E.E., Montes, C., Waite, A.J., 2014. Consequences of shoaling of the Central American Seaway determined from modeling Nd isotopes. Paleoceanography 29. 2013PA002501.
Smith, I.E.M., 1982. Volcanic evolution in eastern Papua. Tectonophysics 87, 315–333.
Soler, P., Rotach-Toulhoat, N., 1990. Sr-Nd isotope compositions of cenozoic granitoids along a traverse of the central Peruvian Andes. Geol. J. 25, 351–358.
Staudigel, H., Doyle, P., Zindler, A., 1985. Sr and Nd isotope systematics in fish teeth. Earth Planet. Sci. Lett. 76, 45–56.
Steinthorsdottir, M., Coxall, H.K., de Boer, A.M., Huber, M., Barbolini, N., Bradshaw, C.D., Burls, N.J., Feakins, S.J., Gasson, E., Henderiks, J., Holbourn, A.E., Kiel, S., Kohn, M.J., Knorr, G., Kürschner, W.M., Lear, C.H., Liebrand, D., Lunt, D.J., Mörs, T., Pearson, P., Pound, M.J., Stoll, H., Strömberg, C.A.E., 2021. The Miocene: the future of the past e2020PA004037 Paleoceanogr. Paleoclimatol.
Sundell, K.E., Saylor, J.E., Lapen, T.J., Horton, B.K., 2019. Implications of variable late Cenozoic surface uplift across the Peruvian central Andes. Sci. Rep. 9, 4877.
Suto, I., Kawamura, K., Hagimoto, S., Teraishi, A., Tanaka, Y., 2012. Changes in upwelling mechanisms drove the evolution of marine organisms. Palaeogeogr. Palaeoclimatol. Palaeoecol. 339–341, 39–51.
Thiel, M., Macaya, E., Acuña, E., Arntz, W., Bastias, H., Brokordt, K., Camus, P., Castilla, J.C., Castro, L., Cortés, M., Dumont, C.P., Escribano, R., Fernández, M., Gajardo, J.A., Gaymer, C., Gómez, I., González, A.E., González, H., Haye, P.A., Illanes, J., Iriarte, J., Lancellotti, D., Luna-Jorquera, G., Luxoro, C., Manríquez, P.H., Marín, V., Muñoz, P., Navarrete, S., Pérez, E., Poulin, E., Sellanes, J., Sepúlveda, H., Stotz, W., Tala, F., Thomas, A., Vargas, C., Vásquez, J.A., Vega, J.A., 2007. The Humboldt Current System of northern and central Chile. Oceanogr. Mar. Biol. Annu. Rev. 45, 195–344.
Thomas, D.J., Via, R.K., 2007. Neogene evolution of Atlantic thermohaline circulation: Perspective from Walvis Ridge, southeastern Atlantic Ocean. Paleoceanography 22, PA2212.
Thouret, J.-C., Wörner, G., Gunnell, Y., Singer, B., Zhang, X., Souriot, T., 2007. Geochronologic and stratigraphic constraints on canyon incision and Miocene uplift of the Central Andes in Peru. Earth Planet. Sci. Lett. 263, 151–166.
Tiedemann, R., Mix, A., 2007. 1. Leg 202 Synthesis: Southeast Pacific paleoceanography. Proceedings of the Ocean Drilling Program, Scientific Results 202, 1–56.
Timmermann, A., An, S.-I., Kug, J.-S., Jin, F.-F., Cai, W., Capotondi, A., Cobb, K.M., Lengaigne, M., McPhaden, M.J., Stuecker, M.F., Stein, K., Wittenberg, A.T., Yun, K.-S., Bayr, T., Chen, H.-C., Chikamoto, Y., Dewitte, B., Dommenget, D., Grothe, P., Guilyardi, E., Ham, Y.-G., Hayashi, M., Ineson, S., Kang, D., Kim, S., Kim, W., Lee, J.-Y., Li, T., Luo, J.-J., McGregor, S., Planton, Y., Power, S., Rashid, H., Ren, H.-L., Santoso, A., Takahashi, K., Todd, A., Wang, G., Wang, G., Xie, R., Yang, W.-H., Yeh, S.-W., Yoon, J., Zeller, E., Zhang, X., 2018. El Niño-Southern Oscillation complexity. Nature 559, 535–545.
Toggweiler, J.R., Druffel, E.R.M., Key, R.M., Galbraith, E.D., 2019. Upwelling in the ocean basins North of the ACC: 1. On the upwelling exposed by the surface distribution of $\Delta^{14}C$. J. Geophys. Res. Oceans 124, 2591–2608.
Tsuchiya, M., Lukas, R., Fine, R.A., Firing, E., Lindstrom, E., 1989. Source waters of the Pacific Equatorial Undercurrent. Prog. Oceanogr. 23, 101–147.
Tütken, T., Vennemann, T.W., Pfretzschner, H.-U., 2011. Nd and Sr isotope compositions in modern and fossil bones – Proxies for vertebrate provenance and taphonomy. Geochim. Cosmochim. Acta 75, 5951–5970.
Vatin-Pérignon, N., Oliver, R.A., Goemans, P., Keller, F., Briqueu, L., Salas, A.G., 1992. Geodynamic interpretations of plate subduction in the northernmost part of the Central Volcanic Zone from the geochemical evolution and quantification of the crustal contamination of the Nevado Solimana volcano, southern Peru. Tectonophysics 205, 329–355.
Villafaña, J.A., Rivadeneira, M.M., 2014. Rise and fall in diversity of Neogene marine vertebrates on the temperate Pacific coast of South America. Paleobiology 40, 659–674.
Von Der Heydt, A.S., Dijkstra, H.A., 2011. The impact of ocean gateways on ENSO variability in the Miocene. Geol. Soc. Lond. Spec. Publ. 355, 305–318.
von Huene, R., Suess, E., Emeis, K.-C., 1987. Convergent tectonics and coastal upwelling: A history of the Peru continental margin. Episodes 10, 87–93.
Wang, D., Gouhier, T.C., Menge, B.A., Ganguly, A.R., 2015. Intensification and spatial homogenization of coastal upwelling under climate change. Nature 518, 390–394.
Watanabe, T., Suzuki, A., Minobe, S., Kawashima, T., Kameo, K., Minoshima, K., Aguilar, Y.M., Wani, R., Kawahata, H., Sowa, K., Nagai, T., Kase, T., 2011. Permanent El Niño during the Pliocene warm period not supported by coral evidence. Nature 471, 209–211.
Zachos, J.C., Pagani, M., Sloan, L., Thomas, E., Billups, K., 2001. Trends, rhythms, and aberrations in global climate 65 Ma to present. Science 292, 686–693.